Geometric Properties of Human Ribs as Predictors of Structural Properties

Michelle M. Murach[1], Michelle Schafman[1], Yun-Seok Kang[1], Susan White[2], John H. Bolte IV[1], Kevin Moorhouse[3], Amanda M. Agnew[1]

[1] The Ohio State University, Injury Biomechanics Research Center

[2] The Ohio State University, Division of Health Information Management Systems

[3] National Highway Traffic Safety Administration, Vehicle Research & Test Center

ABSTRACT

Classification of structural properties of human bones is essential for understanding differential response to loading and fracture risk. Ribs, in particular, are frequently fractured during motor vehicle crashes and are linked to high mortality rates, especially in elderly individuals. While many studies describe variation of bone properties with respect to age and sex differences, these parameters explain only a small amount of variability in rib properties. The focus of this study was to investigate the ability of geometry to predict the response of ribs to dynamic loading.

A total of 122 complete mid-level ribs from 76 fresh post-mortem human subjects (15-99 years of age, 20 females, 56 males) were excised and their span length (Sp.Le) and curve length (Cv.Le) were measured from head to costochondral junction. The ribs were tested in a custom-built pendulum fixture simulating a dynamic frontal impact to the thorax. Peak force (F_{PEAK}) was defined as the maximum force in the primary loading direction prior to failure. Linear structural stiffness (K) was calculated as the slope of 20-80% of the elastic portion of the force-displacement curve. Sections were removed from mid-shaft of the rib and thin-sections were prepared. Cross-sectional microscopic images were obtained at 40x magnification with an Olympus VS120 slide scanner. Measurements were manually made in cellSens Dimension® imaging software (Olympus Corporation) to obtain total subperiosteal area (Tt.Ar) and cortical area (Ct.Ar). Section modulus was calculated for the pleural and cutaneous cortices independently (Z_{PLE} and Z_{CUT}, respectively) in ImageJ software using a customized macro.

Tt.Ar, Ct.Ar, and Z all have positive relationships with F_{PEAK} and K. When considering only cross-sectional geometric values, F was best predicted by Ct.Ar ($p\text{-}R^2=0.673$) and Z_{PLE} ($p\text{-}R^2=0.668$) and K was best predicted by Tt.Ar ($p\text{-}R^2= 0.437$) and Z_{PLE} ($p\text{-}R^2=0.494$). Robusticity, an index used to establish the relationship between longitudinal growth and transverse expansion, allows for the combination of gross and cross-sectional geometric parameters. This index was calculated in four ways: Tt.Ar/Sp.Le, Tt.Ar/Cv.Le, Ct.Ar/Sp.Le, and Ct.Ar/Cv.Le, and these variations were individually evaluated in terms of their ability to predict F_{PEAK} and K. Preliminary findings indicate that F_{PEAK} is best predicted by Ct.Ar/Sp.Le ($p\text{-}R^2=0.709$), but K is best predicted by Tt.Ar/Cv.Le ($p\text{-}R^2=0.784$).

Identifying accurate predictors of structural properties of ribs may improve the ability to assess fracture risk. Additionally, detailed cross-sectional properties can contribute to improved physical and computational models, injury criteria, and clinical assessments of bone fragility.

INTRODUCTION

Ribs are frequently fractured during MVCs and are linked to high mortality rates, especially in elderly individuals (Holcomb et al. 2003; Kent et al. 2008; Sirmali et al. 2003). Although many studies attribute variation in bone properties to age and sex differences, these parameters only explain a small amount of variability in thorax and rib properties (Agnew et al. 2015; Ritchie et al. 2006; Zioupos & Currey 1998; Kent & Patrie 2005). Alternatively, rib geometry may play a crucial role in determining the structural response of the rib to loading, as well as the overall response of the thorax.

Cross-sectional geometric properties can have a significant effect on how a bone will respond to loading. Several studies have investigated variation in material, structural, and geometric properties of ribs with respect to anatomical location and rib level using bending tests of rib sections (Yoganandan & Pintar 1998; Cormier et al. 2005; Kemper et al. 2007; Stein & Granik 1976) or whole ribs (Charpail et al. 2005; Kindig et al. 2011). Results highlight that changes in rib structural properties were accompanied by significant changes in cross-sectional geometry without material property differences. These studies have been limited to a small number of subjects and thus were not able to confidently quantify the strength of relationships between cross-sectional geometric and mechanical properties of ribs.

Whole bone geometry can also play an integral role in determining mechanical properties of bone. Skeletal robusticity (total cross-sectional area relative to bone length) reflects the biological relationship between transverse expansion and longitudinal growth (Jepsen et al. 2013). Bones that fall on the lower end of the robusticity spectrum are referred to as slender, and those that fall on the higher end, robust. Robusticity in bones of the appendicular skeleton has been shown to be related to porosity, cortical tissue mineral density, and tissue modulus, all of which play a critical role in determining whole bone stiffness and strength (Jepsen et al. 2011; Schlecht & Jepsen 2013; Jepsen et al. 2013). However, the relationship between robusticity and mechanical properties has yet to be investigated in the axial skeleton.

There are few studies which directly quantify the role of rib geometry in explaining mechanical properties, although many studies state that geometry *can* influence mechanical properties. The objective of this study is to investigate the ability of gross and cross-sectional geometry to explain variation in measured peak force and linear structural stiffness in whole human ribs.

METHODS

One hundred twenty-two complete mid-level ribs from 76 fresh post-mortem human subjects (20 females, 56 males) were excised from individuals near the time of death (Table 1). Subject ages ranged from 15 to 99 years, with a mean age of 50.9 ± 24.5 years. Ribs were acquired through The Ohio State University's Body Donation Program and Lifeline of Ohio, and their collection was exempted from review by an institutional review board. After procurement, ribs were immediately wrapped in normal saline-soaked gauze and stored at -20°C until testing. Prior to testing, ribs were thawed, all external soft tissue was removed, and the ends potted in

Bondo ® Body Filler (Bondo Corporation, Atlanta, GA). Bondo ® was prepared such that the temperature of the curing Bondo was not greater than approximate body temperature. Total curve length (Cv.Le) and span length (Sp.Le) of each rib were measured from head to costochondral junction (Figure 1). Four strain gages (Vishay Micro-Measurement, Shelton, CT, CEA-06-062UW-350) were applied to the cutaneous and pleural surfaces of each rib at 30% and 60% of Cv.Le to detect time of fracture. Special care was taken to ensure that ribs remained hydrated with normal saline throughout preparation and testing.

Ribs were dynamically tested in a custom-built pendulum fixture based on the design by Charpail et al. 2005. The experiment simulated a frontal impact to the thorax in which the sternal end of the rib was linearly translated toward the vertebral end, creating a 2D bending scenario. Both potted ends of the ribs were fixed in freely rotating cups during the event. A 54.4 kg pendulum impacted ribs at an average velocity of 1-2 m/s. Displacement of the sternal end of the rib was measured by a linear string potentiometer (Rayelco P-20A, AMETEK, Inc. Berwyn, PA) attached to the moving plate of the fixture. Forces were recorded by a 6-axis load cell (CRABI neck load cell, IF-954, Humanetics, Plymouth, MI) located behind the fixed plate. Peak force (F_{PEAK}) was defined as the maximum force in the primary loading direction, X, prior to failure. Linear structural stiffness (K) was calculated as the slope of 20–80% of the elastic portion of the force-displacement curve (see Agnew et al. 2015 for further explanation).

Sections were removed from mid-shaft of the rib (30–70% of Cv.Le) after testing, cleaned of all soft tissue, and embedded in methymethacrylate. Thin-sections (~70 μm) were cut and mounted on slides according to standard histological procedures, and then cross-sectional images were obtained at 40x magnification with an Olympus VS120 slide scanner. Measurements were manually made in cellSens Dimension® imaging software (Olympus Corporation) to obtain total subperiosteal area (Tt.Ar) and cortical area (Ct.Ar) (Figure 1). Section modulus was calculated for the pleural and cutaneous cortices independently (Z_{PLE} and Z_{CUT}, respectively) in ImageJ software (NIH) using a customized macro (Figure 2). Rib robusticity was calculated in four distinct ways: Tt.Ar/Sp.Le, Tt.Ar/Cv.Le, Ct.Ar/Sp.Le, and Ct.Ar/Cv.Le.

A multi-level mixed model was utilized to account for the non-independence of data points, since a varying number of ribs from each subject were tested (Table 1). A pseudo-R^2 (p-R^2) value is used to represent the ability of the independent variable to explain the amount of variance in the dependent variable. The Level 1 model represents the subject-level variables while the Level 2 model represents rib-level variables. For a detailed description of the statistical model, see Agnew et al. 2015. The model was applied to dependent mechanical variables, F_{PEAK} and K, that can be explained by purely cross-sectional geometric variables (i.e., Tt.Ar, Ct.Ar, Z) as well as integrated cross-sectional and whole rib geometry in separate calculations of robusticity (Tt.Ar/Cv.Le, Tt.Ar/Sp.Le, Ct.Ar/Cv.Le, and Ct.Ar/Sp.Le). Each of the cross-sectional geometric and mixed geometric variables was entered into Level 2 models to assess the amount of variation explained in each of the dependent mechanical variables.

Table 1: Subject Demographics

Subject	Sex	Age	Ribs*	Subject	Sex	Age	Ribs*
A5730	M	73	L7	**L12-0037**	M	32	L6
A5891	M	58	R6	**L12-0039**	M	42	R4
A5894	F	92	R5	**L12-0042**	M	53	R4
A5998	M	71	L4, L5	**L12-0045**	M	18	L4
A6011	M	88	R4, R5, R6	**L12-0107**	M	27	L6
A6034	F	80	L4	**L12-0108**	M	42	R3, R5
A6035	M	79	L4, L5, R5, L7	**L12-0132**	M	30	L6
A6047	M	61	R6	**L12-0172**	M	45	R4, R5
A6063	M	82	L7	**L12-0193**	M	48	R5
A6090	F	77	L4, L5, L6	**L12-0214**	M	27	L5, L6
A6141	M	29	R4	**L12-0216**	M	20	L6, R5
A6169	M	67	R4, L5, R5	**L12-0247**	M	48	L4, L6, R6
A6172	M	75	L4, R4, L6, L7, R7	**L12-0252**	M	42	L6
A6233	M	21	L4, R4, L5, R5, L6, R6, L7, R7	**L12-0287**	M	38	R4
A6236	M	69	R4, R5	**L13-0032**	M	30	L5
A6248	M	26	R6	**L13-0216**	F	26	L6, R6
A6281	F	90	L7	**L13-0223**	M	22	L6
A6283	M	85	L6	**L13-0229**	M	32	R7
A6317	M	48	R5	**L13-0252**	M	26	R6
A6327	F	64	L6	**L13-0269**	F	48	R6
A6367	M	84	L5, R5, L7, R7	**L13-0284**	F	51	R6
A6369	F	90	L7	**L13-0325**	M	21	R6
A6390	M	86	L5	**L13-0338**	F	17	L5, R5, L6, R6
A6513	M	67	R6	**L13-0351**	F	24	R6
A6577	F	99	R5	**L13-0352**	M	53	L6
A6583	M	85	R5, R6	**L13-0358**	M	15	R5
A6591	F	92	R7	**L13-0365**	M	44	R6
A6609	M	64	L6	**L13-0374**	M	53	R6, R7
A6613	F	27	L6, R6	**L13-0388**	M	29	L4, L5
A6652	F	88	L7	**L13-0397**	M	22	R5
A6669	M	47	L5	**L14-0021**	M	47	L6
A6717	F	69	L6	**L14-0023**	M	21	L6
A6730	M	33	L6, R6	**L14-0038**	F	18	R5, L6, R6
A6767	F	35	L6, R6	**L14-0044**	F	25	L6
A6802	M	43	L6, R6	**L14-0045**	F	43	R4, R5
L12-1	M	44	R6	**ASM85**	M	76	R6
L12-4	M	51	R4, R6	**ASM93**	M	74	R6
L12-7	M	55	L5, R5	**ASM94**	M	74	R6

* L = left side rib, R = right side rib

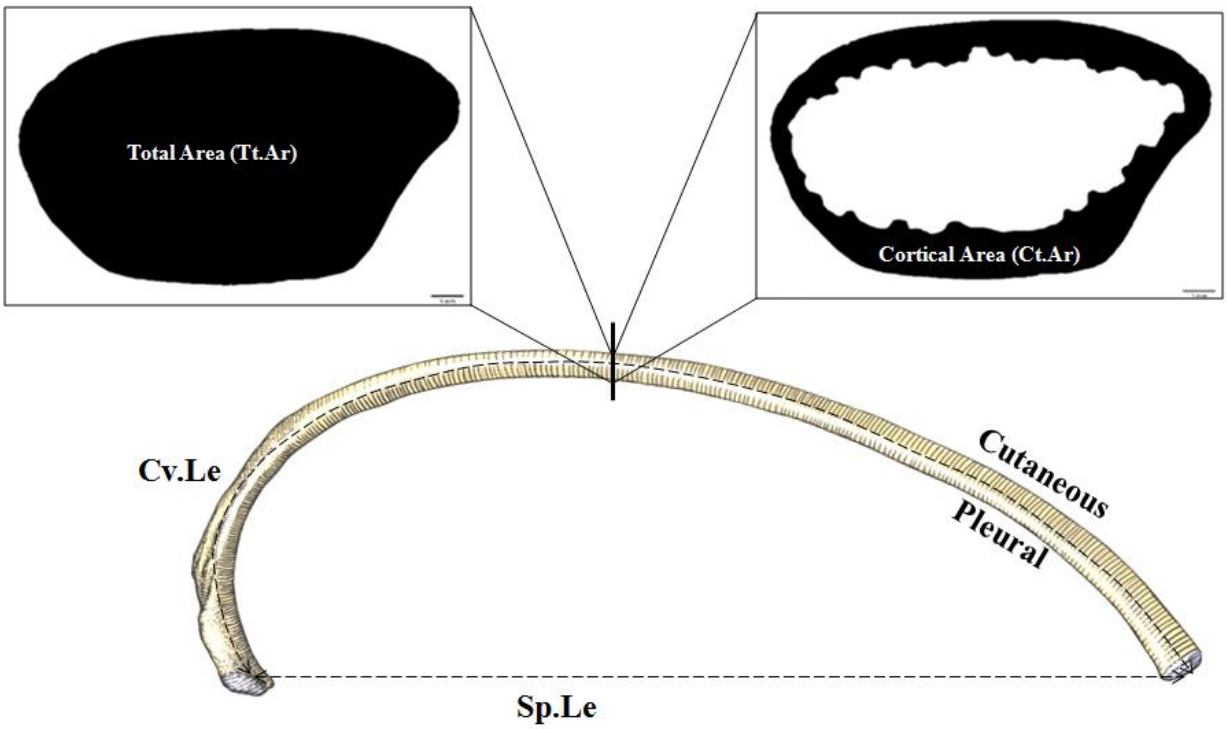

Figure 1. Measurement of Curve Length (Cv.Le), Span Length (Sp.Le) and Cross-Sectional Geometry

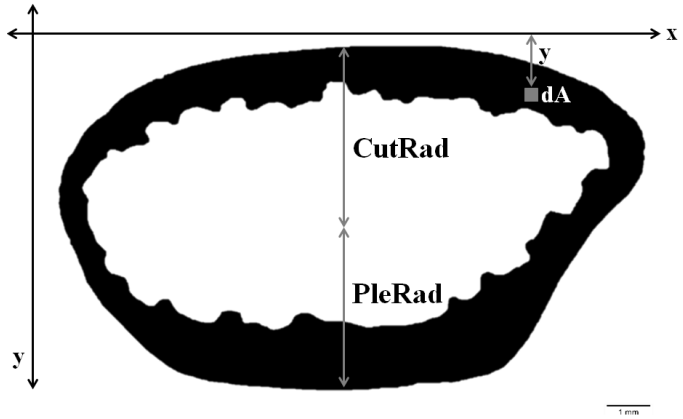

$$I_x = \iint y^2 dA$$

$$Z_{PLE} = \frac{I_x}{PleRad}$$

$$Z_{CUT} = \frac{I_x}{CutRad}$$

Figure 2. Calculations of Section Modulus (Z)

RESULTS

Table 2 displays descriptive statistics for all variables included in this study.

Table 2: Descriptive Statistics

Variable	Mean (±SD)	Min	Max
Tt.Ar (mm^2)	70.19 (±14.69)	33.03	105.81
Ct.Ar (mm^2)	23.90 (±7.02)	9.04	39.56
Z_{PLE} (mm^3)	42.23 (±15.49)	9.81	84.09
Z_{CUT} (mm^3)	40.11 (±15.01)	8.74	77.92
Tt.Ar/Sp.Le (mm)	0.36 (±0.01)	0.16	0.58
Tt.Ar/Cv.Le (mm)	0.25 (±0.05)	0.12	0.39
Ct.Ar/Sp.Le (mm)	0.12 (±0.04)	0.04	0.22
Ct.Ar/Cv.Le (mm)	0.09 (±0.02)	0.03	0.15
F_{PEAK} (N)	115.1 (±44.12)	16.21	242.95
K (N/mm)	3.52 (±1.68)	0.36	9.42

Table 3 highlights the statistically significant ability of all rib geometry to explain variance in peak force (F_{PEAK}) and stiffness (K) (all $p<0.0001$). Total area (Tt.Ar) and cortical area (Ct.Ar) both had statistically significant, positive relationships with F_{PEAK}, although Tt.Ar explains much less variance than Ct.Ar ($p\text{-}R^2 = 0.351$ and $p\text{-}R^2 = 0.673$, respectively) (Figure 3a,b). The use of Tt.Ar in combination with rib span length (Sp.Le) and curve length (Cv.Le) greatly improved the ability to explain the variance in F_{PEAK} compared to Tt.Ar alone ($p\text{-}R^2 = 0.667$ for Tt.Ar/Sp.Le and $p\text{-}R^2 = 0.626$ for Tt.Ar/Cv.Le) (Figure 3c). Combining Ct.Ar with Sp.Le and Cv.Le only improved $p\text{-}R^2$ values slightly, when compared to Ct.Ar alone ($p\text{-}R^2 = 0.709$ and $p\text{-}R^2 = 0.689$, respectively) (Figure 3d).

Table 3: Relationships between geometric and structural properties.*

Variable Type	Independent Variable	Peak Force Pseudo-R^2	Stiffness Pseudo-R^2
Cross-sectional geometry	Tt.Ar (mm^2)	0.351	0.437
	Ct.Ar (mm^2)	0.673	0.259
	Z_{PLE} (mm^3)	0.668	0.494
	Z_{CUT} (mm^3)	0.662	0.433
Mixed geometry (Robusticity)	Tt.Ar/Sp.Le (mm)	0.667	0.694
	Tt.Ar/Cv.Le (mm)	0.626	0.784
	Ct.Ar/Sp.Le (mm)	0.709	0.308
	Ct.Ar/Cv.Le (mm)	0.689	0.327

*The fixed effect for each independent variable was significantly different from zero ($p<0.0001$) for both dependent variables (Peak Force and Stiffness).

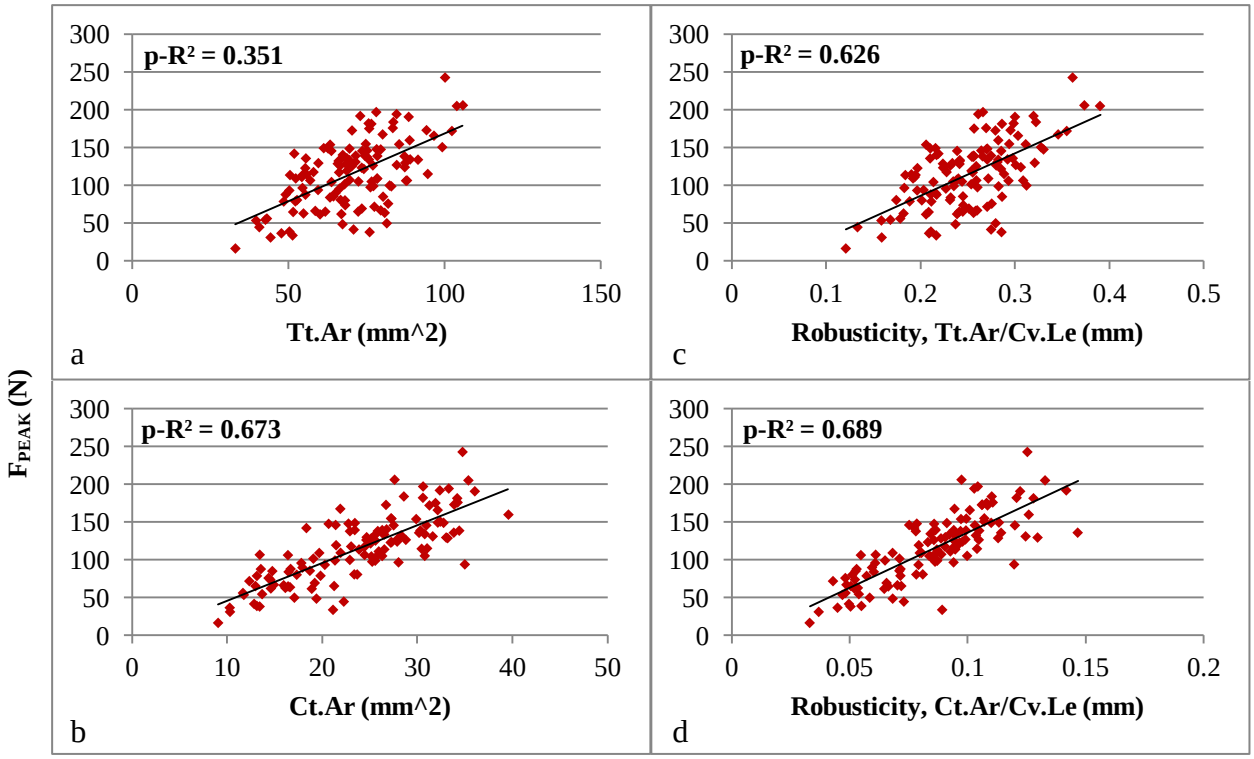

Figure 3. Relationships between geometry and F_{PEAK}. X-axes are individually labeled. Y-axis for all plots is K.

Tt.Ar and Ct.Ar both had statistically significant and positive relationships with K (Figure 4a,b), however, the relationships were not as strong as those with F_{PEAK}. Tt.Ar and Ct.Ar were only able to explain a moderate amount of the variance in K ($p\text{-}R^2$ = 0.437 and $p\text{-}R^2$ = 0.259, respectively). The use of Tt.Ar in combination with Sp.Le and Cv.Le greatly improved the ability to explain the variance in K compared to Tt.Ar alone ($p\text{-}R^2$ = 0.694 for Tt.Ar/Sp.Le and $p\text{-}R^2$ = 0.784 for Tt.Ar/Cv.Le) (Figure 4c). However, combining Ct.Ar with Sp.Le and Cv.Le only improved the relationships slightly, when comparing to Ct.Ar alone ($p\text{-}R^2$ = 0.308 for Ct.Ar/Sp.Le and $p\text{-}R^2$ = 0.327 for Ct.Ar/Cv.Le) (Figure 4d).

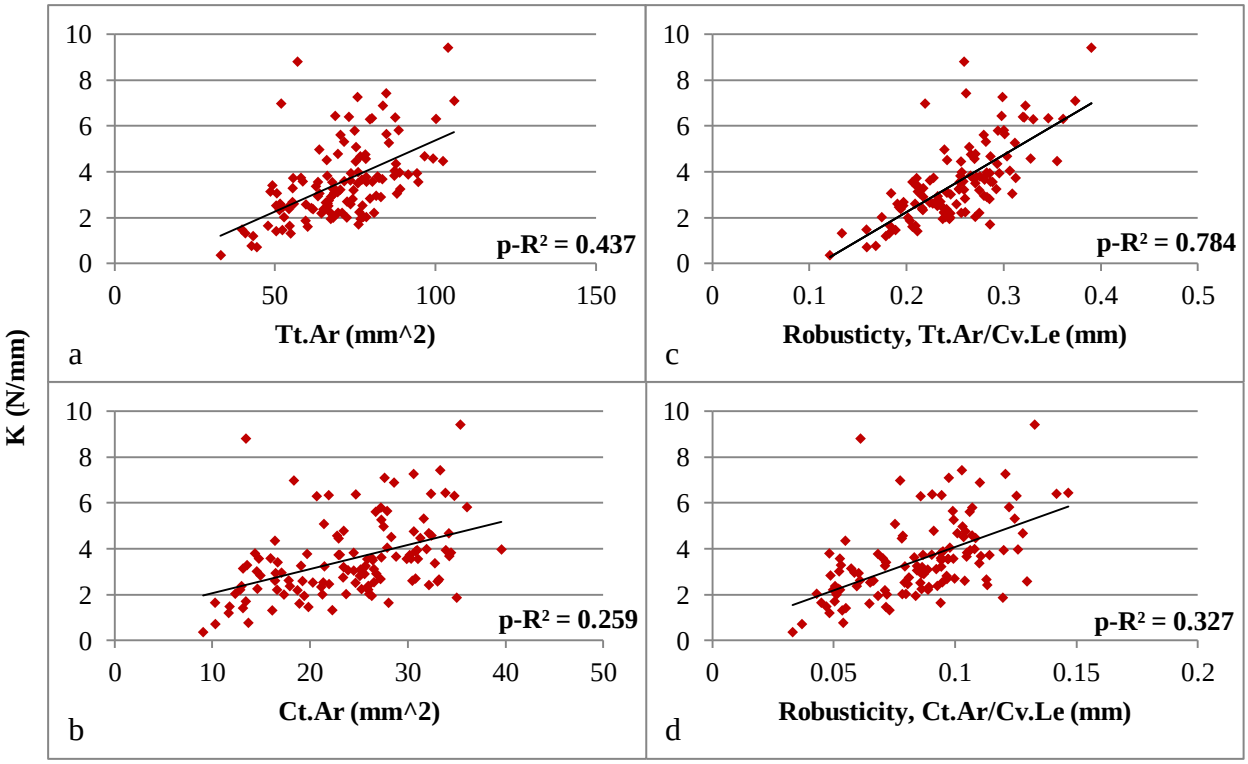

Figure 4. Relationships between geometry and K. X-axes are individually labeled. Y-axis for all plots is K.

DISCUSSION

Relationships observed in this study indicate cross-sectional geometric properties are important for understanding the maximum force a rib can withstand prior to fracture. All relationships between cross-sectional geometry, robusticity, and peak force were found to be statistically significant and positive, indicating that ribs with greater cross-sectional properties, and those that are more robust, are able to withstand higher forces. Ct.Ar was better able to account for variation in F_{PEAK} than Tt.Ar, which could be attributed to the amount of cortical bone, not the overall size, being the primary load bearing aspect of the ribs (Figure 3a,b). Interestingly, the integration of gross geometry by utilizing robusticity as a predictor of F_{PEAK} only slightly improved relationships compared to cross-sectional geometry alone when Ct.Ar was used in the calculations, but greatly improved the relationship when Tt.Ar was used (Figure 3c,d). Ultimately all robusticity calculations performed equally well and there was little difference between robusticity calculated with Cv.Le and Sp.Le in the ability to predict peak force.

Cross-sectional geometry alone is not sufficient to describe variability in stiffness. Tt.Ar, Ct.Ar, and Z were only able to explain a moderate amount of variation in stiffness (Figure 4a,b). However, the addition of the overall size of the rib by incorporating Cv.Le and Sp.Le into calculations of robusticity, improved relationships between stiffness and geometric properties. It should be noted that robusticity calculations utilizing Ct.Ar were not as successful at predicting

stiffness as those using Tt.Ar, which parallels the relationships seen when using cross-sectional geometry alone (Figure 4). With 78.4% of the variation in stiffness explained by robusticity calculated as Tt.Ar/Cv.Le, structural stiffness is highly dependent on the overall size and shape of the rib.

The trends reported here for cross-sectional geometry and structural properties are comparable with those reported in other studies (Yoganandan & Pintar 1998; Cormier et al. 2005; Kemper et al. 2007; Charpail et al. 2005; Kindig et al. 2011; Sedlin et al. 1963; Stein & Granik 1976). Yoganandan and Pintar (1998) conducted quasi-static three-point bending tests on 7^{th} and 8^{th} ribs and found differences in cross-sectional geometry but not mechanical properties. However, Cormier et al. (2005) tested samples from ribs 2-12 in three-point bending and found significant differences in mechanical properties with respect to geometry. Results highlighted positive relationships between cross-sectional and mechanical properties similar to those shown here, but trends were weak due to a limited number of subjects. Kemper et al. (2007) also investigated geometric, material, and mechanical properties from dynamic bending tests and found no significant differences with respect to material properties, but that changes in structural response were accompanied by significant changes in cross-sectional geometry. Additionally, the strong dependence of F_{PEAK} on Ct.Ar and K on Tt.Ar demonstrated here are similar to findings of Perz et al. (2015).

Robusticity is frequently applied to long bones of the appendicular skeleton to predict material and mechanical properties (Jepsen et al. 2011; Schlecht & Jepsen 2013). However, the unusual geometry of the rib makes robusticity in the classical sense, a simple relationship between transverse expansion and longitudinal growth, difficult to define. Robusticity was calculated in four distinct ways here, utilizing Tt.Ar, Ct.Ar, Cv.Le, and Sp.Le, to investigate the ability of the combination of gross and cross-sectional geometry to explain variation in structural properties of the rib. Figures 3 and 4 indicate these combinations representing the overall geometry of the rib are valuable tools for estimating mechanical properties. Robusticity has added value due to the potential ability of obtaining the required variables from a clinical CT, particularly in calculations utilizing Tt.Ar and Sp.Le.

The ability to explain variation in structural stiffness of the ribs utilizing robusticity has great potential for aiding in ATD design improvements and validation of computational models of the human thorax. The results presented here can be used to help bridge the gap between rib geometry and response and its relation to overall thorax geometry and response to loading, which could ultimately improve injury criteria. Furthermore, an understanding of the combination of gross and cross-sectional geometry and its ability to predict structural stiffness may also improve chest deflection corridors, which are used to determine thoracic injury risk (Kroell et al. 1971; Nahum et al. 1975; Viano 1978; Morgan et al. 1994; Kent et al. 2001a; Kent et al. 2001b; Kent & Patrie 2005).

Although the results of this study are a critical first step in the investigation of the influence of rib geometry on structural properties, there are still several limitations. Cross-sectional geometry and robusticity were not explored with respect to age, sex, or BMI, which could play a role in the determination of these properties. Additionally, ages and sexes are not equally represented in the sample, so some bias may exist.

CONCLUSIONS

- Cortical area proved to play an important explanatory role for peak force. Robusticity utilizing total area was found to be more useful in explaining structural stiffness.
- All relationships were statistically significant and positive, indicating ribs with larger cross-sectional properties and those that are more robust have a greater ability to resist fracture, similar to long bones.
- Cross-sectional and gross geometric properties of human ribs play an important role in determining response to loading and possibly fracture risk. These data can be utilized to improve the biofidelity of ATDs and the accuracy of physical and computational models of the human thorax.

ACKNOWLEDGEMENTS

Funding for this study was provided by National Highway Traffic Safety Administration (NHTSA). Thank you to Timothy Gocha and Victoria Dominguez for preparing and imaging ribs. Thank you to all of the students and staff of the Injury Biomechanics Research Center, especially HyunJung Kwon, Kyle Icke, Julie Bing, Allison Guettler, and Randee Hunter for their endless support. Thank you to Rod Herriott and Patrick Brown from the Transportation Research Center, Inc. and Jason Stammen and Bruce Donnelly from NHTSA. Thank you to Mark and Michelle Whitmer, OSU's Body Donor Program, Lifeline of Ohio, and especially the donors for their generous gifts.

REFERENCES CITED

Agnew, A.M. et al., 2015. The effect of age on the structural properties of human ribs. *Journal of the Mechanical Behavior of Biomedical Materials*, 41, pp.302–314.

Charpail, E. et al., 2005. Characterization of PMHS Ribs; A New Test Methodology. *Stapp Car Crash Conference*, 49, pp.183–198.

Cormier, J.M. et al., 2005. Regional Variation in the Structural Response and Geometrical Properties of Human Ribs. *Association for the Advancement of Automotive Medicine*, 49, pp.153–170.

Holcomb, J.B. et al., 2003. Morbidity from Rib Fractures Increases after Age 45. *Journal of the American College of Surgeons*, 196(4), pp.549–555.

Jepsen, K.J. et al., 2011. Biological Constraints That Limit Compensation of a Common Skeletal Trait Variant Lead to Inequivalence of Tibial Function Among Healthy Young Adults. *Journal of Bone and Mineral Research*, 26(12), pp.2872–2885.

Jepsen, K.J. et al., 2013. Variation in Tibial Functionality and Fracture Susceptibility Among Healthy, Young Adults Arises From the Acquisition of Biologically Distinct Sets of Traits. *Journal of Bone and Mineral Research*, 28(6), pp.1290–1300.

Kemper, A.R. et al., 2007. The Biomechanics of Human Ribs: Material and Structural Properties from Dynamic Tension and Bending Tests. *Stapp Car Crash Journal*, 51(October), pp.235–273.

Kent, R. & Patrie, J., 2005. Chest deflection tolerance to blunt anterior loading is sensitive to age but not load distribution. *Forensic Science International*, 149(2-3), pp.121–128.

Kent, R., Woods, W. & Bostrom, O., 2008. Fatality risk and the presence of rib fractures. *Annals of Advances in Automotive Medicine*, 52(October), pp.73–82.

Kent, R.W., Bolton, J.R. & Crandall, J.R. 2001a. The influence of superficial soft tissues and restraint condition on thoracic skeletal injury prediction. *Stapp Car Crash Journal*, 45, pp.183–203.

Kent, R.W., Bolton, J.R. & Crandall, J.R. 2001b. Restrained Hybrid III dummy-based criteria for thoracic hard tissue injury prediction. In *International Conference on the Biomechanics of Impact*. pp.215–232.

Kindig, M., Lau, A.G. & Kent, R.W., 2011. Biomechanical Response of Ribs Under Quasistatic Frontal Loading. *Traffic Injury Prevention*, 12(4), pp.377–387.

Kroell, C., Schneider, D. & Nahum, A., 1971. Impact tolerance and response of the human thorax. In *Society of Automotive Engineers*. p. Paper 710851.

Morgan, R.M. (NHTSA) et al., 1994. Thoracic Trauma Assessment Formulations for Restrained Drivers in Simulated Frontal Impacts. In *Stapp Car Crash Conference*, 38, pp.15–34.

Nahum, A., Schneider, D. & Kroell, C., 1975. Cadaver skeletal response to blunt thoracic impact. In *Stapp Car Crash Conference*. pp.259–293.

Perz, R., Toczyski, J. & Subit, D., 2015. Variation in the human ribs geometrical properties and mechanical response based on X-ray computed tomography images resolution. *Journal of the Mechanical Behavior of Biomedical Materials*, 41, pp.292–301.

Ritchie, R.O. et al., 2006. Fracture and Ageing in Bone: Toughness and Structural characterization. *Strain*, 42(4), pp.225–232.

Schlecht, S.H. & Jepsen, K.J., 2013. Functional integration of skeletal traits: An intraskeletal assessment of bone size, mineralization, and volume covariance. *Bone*, 56(1), pp.127–138.

Sedlin, E.D., Frost, H.M. & Villanueva, A.R., 1963. Variation in Cross-Section Area of Rib Cortex with Age. *Journal of Gerontology*, 18(1), pp.9–13.

Sirmali, M. et al., 2003. A comprehensive analysis of traumatic rib fractures: Morbidity, mortality and management. *European Journal of Cardio-thoracic Surgery*, 24(1), pp.133–138.

Stein, I.D. & Granik, G., 1976. Rib structure and bending strength: an autopsy study. *Calcified Tissue Research*, 20(1), pp.61–73.

Viano, D., 1978. Thoracic Injury Potential. In *International Conference on the Biomechanics of Impact*. pp.142–156.

Yoganandan, N. & Pintar, F.A., 1998. Biomechanics of Human Thoracic Ribs. *Journal of Biomechanical Engineering*, 120(1), pp.100–104.

Zioupos, P. & Currey, J.D., 1998. Changes in the Stiffness, Strength, and Toughness of Human Cortical Bone With Age. *Bone*, 22(1), pp.57–66.